

Foamed concrete produced from CO₂/N₂ foam stabilized by CaCO₃ nanoparticles and CTAB



Ahmed G. Mehairi ^a, Rahil Khoshnazar ^{b,*}, Maen M. Husein ^{a,*}

^a Department of Chemical and Petroleum Engineering, University of Calgary, 2500 University Dr NW, Calgary, AB T2N 1N4, Canada

^b Department of Civil Engineering, University of Calgary, 2500 University Dr NW, Calgary, AB T2N 1N4, Canada

ARTICLE INFO

Keywords:
 Nanoparticle
 Foamed concrete
 CaCO₃
 CO₂
 Compressive strength
 Thermal insulation

ABSTRACT

Foamed concrete (FC) has garnered popularity, especially with the growing demand for energy-efficient and sustainable construction materials. The stability of the FC slurry as it sets is crucial to the uniformity of the pore structure and, subsequently, FC performance. This study investigates the stability of a novel FC produced using aqueous CaCO₃ nanoparticle (NP)/hexadecyltrimethylammonium bromide (CTAB) foam. The effect of NPs and gas type (pure N₂, pure CO₂, and a 2:1 gas mixture of CO₂/N₂) on the FC dry density, compressive strength, water absorption, macro- and microstructure, hydration products, and thermal insulation is explored. The results show that the dry density of FC increases with the inclusion of CO₂ owing to gas liberation during mixing with the paste leading to less voids. Using the gas mixture, CaCO₃/CTAB foam increases the compressive strength of the FC by 38% compared with CTAB alone owing to enhanced uniformity of the pore structure and a denser hydrated paste skeleton. Such structure leads to less connected pores, which reduces atmospheric carbonation, and improves thermal insulation performance. A 2-fold decrease in the largest pore size and a 25% decrease in surface temperature when exposed to an open flame are also achieved in the presence of CaCO₃ NPs.

1. Introduction

Given the construction industry's growing emphasis on sustainability and energy efficiency, the utilization of FC has been the focus of several recent studies due to its low density and outstanding sound and thermal insulation properties [1–4]. FC is a type of cellular lightweight concrete characterized by a porous structure formed by introducing gas bubbles into fresh cement pastes or mortars [5–7]. Owing to its porous structure, FC has low density, high strength/weight ratio, low thermal conductivity, excellent fire resistance, and good sound absorbance [8,9]. Moreover, FC slurry is a self-leveling free-flowing material that can be made with a wide range of densities making it a versatile lightweight material suitable for diverse applications [10,11]. FC with low densities (300 – 600 kg/m³) is typically used for thermal and acoustic insulation and fire protection while FC with densities of 700 – 1100 kg/m³ is commonly used for brick manufacturing and nonstructural components such as divisions and floor leveling mortars [12,13]. Structural components such as load supports and slabs can also be made from higher density FC (1200 – 1800 kg/m³) [12,13]. FC is also used for road sub-base, bridge abutments, trench reinstatement, soil stabilization and shock absorbing barriers [7]. Nevertheless, especially at low densities,

FC displays key drawbacks such as low compressive strength, high shrinkage, high risk of cracking, pore structure instability, high water absorption, and high permeability, which limit its applicability [14–16].

FC properties are directly dependent on the paste/mortar composition and its pore structure [11,17,18]. FC functionality and properties can be altered through the use of various binder materials, including Portland cement, magnesium phosphate cement, calcium sulphoaluminate cement, high alumina cement and geopolymers [13,19,20]. Other supplementary materials and fillers such as silica fume, limestone, fly ash, and blast furnace slag in addition to polymers, plastic waste, fibers, and recycled concrete have also been incorporated into the FC mix design to improve FC properties and/or reduce its cost [12,19,21,22]. Additionally, the FC pore structure is highly dependent on the method of production and type of foaming agent [23,24]. The entrainment of gas voids within fresh pastes and mortars is accomplished through chemical or physical (mechanical) foaming methods. In the chemical methods, the cellular structure of FC is formed by the gas produced from the reaction of precursors with cement hydration products (e.g., reaction of alumina powder and Ca(OH)₂ yielding H₂ [25]) or with each other during slurry mixing and curing. She et al. [26], for instance, prepared white Portland cement FC by adding H₂O₂ solution into a cement paste

* Corresponding authors.

E-mail addresses: rahil.khoshnazar@ucalgary.ca (R. Khoshnazar), maen.husein@ucalgary.ca (M.M. Husein).

containing manganese (Mn) and calcium stearate. The decomposition of H_2O_2 in the presence of Mn produced O_2 bubbles that were then stabilized by calcium stearate. Physical foaming entails either addition of foaming agents to cement pastes coupled with high shear mixing to entrap bubbles (mixing method) or mixing cement pastes with preformed aqueous foams (preformed foam method) [27]. Although the preformed foam method might be operationally more challenging than the mixing method (a stable foam needs to be created independent of the cement paste or mortar), it requires less foaming agent and leads to a more stable and refined void structure [12,13,25]. Accordingly, the stability of the preformed foam is of paramount importance [17,18,28].

The inclusion of NPs in FC has been found to improve the fresh and hardened properties of FC [12,13,29]. NPs can be incorporated into the FC structure either through the cement paste or the preformed foam. The first approach involves preparing the cement paste with the NPs already dry blended with the solid content (i.e., cement and any fillers) [15] or dispersed within the mix water of the paste [26,30]. The preformed foam approach requires the addition of NP-stabilized aqueous foam to the cement paste to produce the FC slurry [10]. This approach targets the stabilization of the bubble structure during foam generation, mixing with the paste, and within the fresh FC slurry as it sets. NPs have been found to stabilize aqueous foams through adsorption at the gas-liquid interface (e.g., partially hydrophobic NPs) and/or stratification (e.g., hydrophilic NPs), leading to the formation of a network structure that decreases liquid drainage and sterically hinders bubble coalescence and coarsening [31,32]. Recent studies have investigated the structure and properties of FC made from preformed foam stabilized with different types of NPs including SiO_2 [5,10,11,33–39], Al_2O_3 [14,40,41], carbon dots [42], TiO_2 [43], ferrous–ferric oxide [44], Fe_3O_4 [45] and potato starch [46]. Foams stabilized with an optimum content of SiO_2 NPs led to a homogenous pore size distribution within the FC [33]. Moreover, compared to FC without NPs, FC made with foams stabilized with Janus SiO_2 NPs showed higher compressive strength across a range of densities due to smaller and more uniform pore sizes as reported by Du et al. [10]. In that study, lower thermal conductivities of the SiO_2 NP-stabilized FC were reported across all tested densities compared to the reference FC. FC was also prepared with densities as low as 80 kg/m^3 with a thermal conductivity comparable to that of organic thermal insulation materials such as expanded and extruded polystyrene [10]. At such low densities, FC can be an attractive thermal insulation material compared to organic insulation materials since FC has higher fire resistance [26,47,48]. Furthermore, FC produced from carbon dots stabilized foam exhibited 30% reduction in thermal conductivity than the reference FC due to smaller and more uniform pore size distribution [42]. Less drying shrinkage, enhanced compressive strength and a uniform FC structure were also achieved in the presence of Al_2O_3 NPs along with synthetic- and protein-based surfactants [14].

CaCO_3 NPs are among the least expensive and widely produced NPs [49]. The effect of CaCO_3 NPs on the mechanical properties and microstructure of conventional cement-based materials has been studied by several researchers [50,51]. However, literature on the effect of CaCO_3 NPs on FC properties is limited. Mydin et al. [15] has recently studied the effect of CaCO_3 NPs on FC properties by dry blending the NPs with solids (cement and sand) and utilizing protein-based preformed foam. They reported that the presence of CaCO_3 NPs promoted the formation of a compact FC matrix with small pore sizes leading to improved compressive, tensile, and flexural strengths. Deterioration of mechanical performance was, however, observed at NPs content above 4 wt% due to NP agglomeration within the mortar. In addition, protein-based foaming agents may suffer from composition inconsistency, limited storage life, and complex manufacturing process compared with synthetic surfactants [52]. Using preformed foam stabilized by micro-waste limestone powder (CaCO_3 and dolomite), synthetic anionic surfactant, and a synthetic polymer, FC showed higher stability and strength than in absence of limestone powder [53].

Prior art on FC made of CaCO_3 NP-stabilized preformed foam is

scarce. The utilization of these NPs in FC was restricted to the dry blending approach in conjunction with a preformed foam stabilized solely by protein-based foaming agents [15]. To fill this gap, this study investigated the stability of FC produced from Portland cement paste and aqueous foams stabilized only by CaCO_3 NPs and a synthetic surfactant (CTAB). Moreover, most FC studies focus on preformed foam made with compressed air, while literature on FC made with CO_2 preformed foam is limited [54–56]. To examine the CO_2 capture prospects of FC, the preformed foam was made using N_2 , CO_2 , and a mixture of both. Furthermore, the CaCO_3 NPs were produced using Ca(OH)_2 carbonation, a CO_2 capture method [57], as detailed in our earlier study [58]. The effect of the CaCO_3 NP-stabilized foam and gas type on the compressive strength, water absorption, pore structure, and thermal insulation of FC were also examined.

2. Materials and methods

2.1. Materials

Portland cement (Quikrete, Canada) complying with the Canadian Standard (CSA A3001) for type GU/GUL was used in preparing the cement pastes. The chemical composition of the cement as obtained by X-ray fluorescence spectroscopy (XRF) is shown in Table 1. Powder Ca(OH)_2 (purity > 95%) procured from Thermo Fisher Scientific (USA) was used to synthesize the CaCO_3 NPs. CTAB (purity ≥ 99.0%, CMC = 0.92 mM) was supplied by MilliporeSigma (Canada). N_2 (99.9% pure) and CO_2 (99.9% pure) gases were purchased from Air Liquide (Canada) and Praxair (Canada), respectively.

2.2. Experimental methods

2.2.1. Preparation of CaCO_3 NPs, CaCO_3 /CTAB dispersions and CTAB solution

CaCO_3 NPs were synthesized by Ca(OH)_2 carbonation at atmospheric pressure and room temperature according to the overall carbonation reaction (R1). CO_2 gas was bubbled within an aqueous suspension of 1 M Ca(OH)_2 until reaching a pH of ~7 – 8. The NP suspension was filtered, and then, the NPs were washed and dried. The CaCO_3 NPs/CTAB dispersions were prepared by dispersing CaCO_3 in distilled water using sonication and then adding CTAB. For the CTAB solution without NPs, a certain amount of CTAB was dissolved in distilled water using a magnetic stirrer. More details on the synthesis process can be found in our earlier study [58].



2.2.2. Preparation of preformed foam and foamed concrete

Cement paste was made by mixing cement and distilled water in a paddle mixer (Kitchen Aid, USA) for 2 min. The water to cement ratio (w/c) for the cement paste was kept constant at 0.4 for all samples (Table 2). While the paste was being mixed, a foam was generated using the setup presented in Fig. 1. The foaming solution/dispersion was fed into a porous medium using a diaphragm pump (DDP 5800, Aquatic, USA) at a rate of $1400 \text{ cm}^3/\text{min}$. Gas (N_2 , CO_2 , or 1:2 mixture of the two) was injected simultaneously. The total gas flowrate was calibrated to achieve a target foam density of 0.1 g/cm^3 . The porous medium consisted of a PVC pipe (length: 34.4 cm, ID: 3.5 cm) packed with stainless steel spiral wire leading to a porosity of 91%. The inlet to the porous medium was a LLDPE tube (ID: 0.6 cm) and the outlet was attached to a nozzle (length: 2.5 cm, outlet ID: 2.1 cm). The foam was collected in a glass beaker and weighed to measure density. The foam was then added gradually to the initial paste, while being mixed, within a time span of 1 min. The mixing continued for 2 – 3 min until a homogeneous slurry was obtained (Figure S1). The stability of the preformed foam during the different stages of the FC production process is an important factor that affects the FC dry density and the stability [17,18]. To better

Table 1

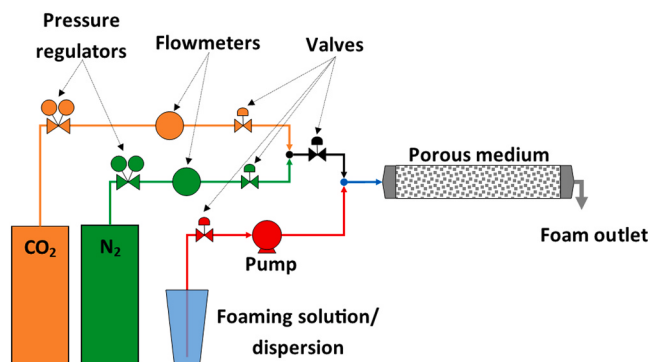
Chemical composition of the cement (wt%).

CaO	SiO ₂	Al ₂ O ₃	Fe ₂ O ₃	MgO	SO ₃	K ₂ O	Na ₂ O	Others	Loss on Ignition
60.15	18.29	3.79	3.32	4.53	3.29	0.39	0.12	6.12	5.89

Table 2

Mixture proportions of FC samples tested in this study.

Sample	Preformed foam				Initial paste mix		Foamed concrete				
	Gas type	CaCO ₃ NPs content, wt% of dispersion	CTAB concentration, wt% of dispersion	Foam density, g/cm ³	Cement, g	Water, g	Added foam volume, cm ³	Final w/c ratio ¹	Average 48-h density ² , g/cm ³	Average 28-day density ³ , g/cm ³	CaCO ₃ NPs content, wt% of cement ⁴
CS	N ₂	0	0.05	0.11	500	200	1111	0.63	0.52 ± 0.10	0.52 ± 0.10	0
CS	CO ₂ /N ₂	0	0.05	0.10	500	200	1111	0.63	0.87 ± 0.09	0.85 ± 0.07	0
CS	CO ₂ /N ₂	0	0.05	0.12	500	200	1226	0.70	1.51 ± 0.13	1.27 ± 0.11	0
NP ₁	CO ₂ /N ₂	1	0.05	0.10	500	200	1111	0.62	0.86 ± 0.09	0.77 ± 0.11	0.2
NP ₃	CO ₂ /N ₂	3	0.05	0.10	500	200	1111	0.61	0.84 ± 0.09	0.84 ± 0.09	0.7
NP ₅	N ₂	5	0.05	0.11	500	200	1111	0.63	0.53 ± 0.05	0.53 ± 0.04	1.2
NP ₅	CO ₂ /N ₂	5	0.05	0.10	500	200	1111	0.62	0.86 ± 0.03	0.85 ± 0.02	1.1
NP ₅	CO ₂	5	0.05	0.11	500	200	1226	0.65	1.47 ± 0.04	1.29 ± 0.03	1.3

¹ Final w/c ratio includes the water contribution from the foam and the initial cement paste.² 48-h density refers to the density of the cubes right after demolding (48 h from casting) and before placement in the moist room.³ 28-day density refers to the density of the cubes after drying at room temperature and 40–60% relative humidity for 3 days (end of the 28 days curing procedure).⁴ Assuming CaCO₃ NPs content in the liquid part of the foam is the same as that of the foaming dispersion.**Fig. 1.** Foam generation setup.

understand the impact of gas type, all samples were produced using the same quantities of Portland cement, water, and foam (**Table 2**). The FC samples made with CO₂ alone had a slightly higher foam volume to ensure that sufficient slurry was available for at least three cubes due to the high instability of the CO₂ foam [58].

The foamed slurry was cast in cubical molds (5×5×5 cm³) and covered with a plastic wrap to prevent water evaporation. During casting, a thin steel rod was used to slightly tap the corners of the molds from the inside to ensure proper filling. The cubes were de-molded after 2 days and stored in a moist room with a relative humidity (RH) over 95% for 23 days. The cubes were then left at room temperature with a RH between 40–60% for 3 days. The curing procedure was performed according to ASTM C495/C495M [59] and lasted a total of 28 days. Throughout this manuscript, the terms “top” and “bottom” sections of the cubes refer to the original orientation of the cubes inside the molds during casting and curing.

2.2.3. FC characterization

The density of the FC samples was determined from the volume of the cubes and their weight after 48 h and 28 days. The cube volume was

calculated from the measured cube dimensions via a digital caliper (Mastercraft, Canada). The average density was obtained from six cubes for pure N₂ and the gas mixture while it was determined from three cubes for pure CO₂ samples. The compressive strength was measured from three 5×5×5 cm³ FC cubes after 28 days using an axial compression machine (Riehle, USA). The orientation of the FC cubes during testing is shown in **Figure S2** of the Supporting Material. Water absorption was determined according to ASTM C796 [60] from three 5×5×5 cm³ FC cubes instead of cylindrical samples. After the 28-day curing period, the cubes were submerged 150 mm below the water surface for 24 h. The cubes were then removed, and excess water was allowed to drain for 30 s before weighing the cubes. The difference in mass before and after water submersion was used to calculate the absorbed water volume.

Pore size distribution was estimated using an image processing software (ImageJ) from images that covered an area of 2.5×2.5 cm² taken via a CMOS 12MP camera. Pores with diameter < 0.1 mm were discarded and considered noise at that magnification.

Microstructure characterization was performed using scanning electron microscopy (SEM) (Quanta FEG 250, FEI, USA, and Phenom ProX, Phenom World, Netherlands) equipped with energy dispersive X-ray (EDX). The SEM samples were FC chips from the top and bottom sections of cubes used for compressive strength testing. In addition to the EDX insights, compositional analysis was performed using simultaneous thermogravimetry analysis (STA) and X-ray diffraction (XRD) on ground FC samples. STA was conducted using TGA/DSC 3+ (Mettler Toledo, Switzerland) coupling both thermogravimetry analysis (TGA) and differential scanning calorimetry (DSC). The temperature of all samples was raised from 25 °C to 1000 °C at 10 °C/min under 50 mL/min of N₂ gas. The amounts of Ca(OH)₂ and CaCO₃ were estimated from the TGA mass loss at 400–500 °C and 500–800 °C, respectively, using the tangential method described in [61]. XRD was performed in a D8 ADVANCE ECO diffractometer (Bruker, USA). Corundum was used as an internal reference. The data were collected in a 2θ range of 5–90° with a 2θ step size of 0.013° and a step time of 0.56 s per step.

Heat of hydration was measured using an isothermal calorimeter

(TAM Air 8-channel, TA Instruments, USA) at 25 °C. The paste was prepared by mixing 0.05 wt% CTAB solution or 5 wt% CaCO₃/0.05 wt% CTAB dispersion with the cement. A w/c of 0.6 was selected based on the expected w/c after mixing with the foam. After placing the required amount of paste inside the ampoule, gas (pure N₂, pure CO₂, or a mixture of both) was injected inside the ampule to displace air in order to investigate the effect of gas type on cement hydration.

Thermal insulation was tested using the setup in Fig. 2a. A heating plate (Chemglass Life Sciences, USA) was covered in insulation (ceramic fiber) except 5×5 cm² area where the cubes were placed sideways to better test the effect of FC instability on heat transfer. The cubes were also surrounded by insulation on all sides except the surface that was in contact with the hot plate and the surface where the thermocouples were attached. The thermocouples were placed at the top and bottom sections of the cubes inside 5 mm (depth) holes so that the thermocouple tips were surrounded by the FC matrix for more accurate temperature readings. The heating plate temperature was set at 35, 60 and 90 °C. At each temperature setting, temperature readings for the top and bottom of each cube were recorded every minute for a total of 1 h as no significant change in temperature was observed beyond 1 h. Furthermore, thermal insulation was also tested in the presence of fire using a propane torch as seen in Fig. 2b. The outlet of the torch was placed 3 cm from the cube surface [10], and thermocouples were attached to the opposite end of the cube. The exposure to flame continued for 5 min and the highest temperature reading was recorded.

3. Results and discussion

Characterization of the CaCO₃ NPs and CaCO₃/CTAB dispersion, static foam stability tests and foam stability mechanisms were detailed in our previous publication [58]. The produced NPs were found to be calcite with an average particle size of 72 ± 19 nm according to Fourier transform infrared (FTIR) spectra and transmission electron microscopy (TEM) micrographs. Aqueous foams made with CaCO₃ NPs/CTAB dispersions showed higher static stability than CTAB alone independent of the gas phase. Moreover, foams made with pure CO₂ were much less stable than those made with pure N₂ or a gas mixture (2:1 CO₂/N₂) regardless of the foaming solution/dispersion composition. In presence of the gas mixture, the highest static stability and smallest bubble sizes were achieved using 5 wt% CaCO₃ NPs/CTAB dispersion while the lowest static stability and largest bubble sizes resulted from CTAB alone.

3.1. Density and stability of FC structure

Fig. 3 displays the variation of FC 48-h and 28-day densities with gas type in absence (CS) and presence of 5% (based on the foaming dispersion mass) CaCO₃ NPs (NP₅). For the 2:1 CO₂/N₂ gas mixture, FC samples made with preformed foams containing 1% (NP₁) and 3% (NP₃)

CaCO₃ NPs (based on the foaming dispersion mass) were also tested. The FC samples prepared with pure N₂ showed the least densities (520 – 530 kg/m³) among all samples. Both the 48-h and the 28-day densities of FC increased with increasing the CO₂ content in the foaming gas. For a 2:1 CO₂/N₂ gas mixture, the density increased to 840 – 850 kg/m³. The FC density leaped to 1280 – 1290 kg/m³ with pure CO₂, despite the addition of more foam. The density of the produced FC was highly dependent on the amount gas entrapped within the foamed slurry and the inclusion of NPs did not show any significant impact on the overall FC density.

The variation in density of the FC is in line with the stability of the preformed foam. Aqueous foams destabilize through several mechanisms including liquid drainage, coarsening and coalescence [62,63]. Coarsening (Ostwald ripening) occurs when the gas diffuses from smaller to larger bubbles due to the Laplace-Young capillary effect [62, 64–66]. Since CO₂ is more soluble in aqueous solutions than N₂, CO₂ aqueous foams are far less stable and experience a higher rate of Ostwald ripening [67]. In this study, the preformed foams underwent vibrations and disturbances during generation, collection, transportation to the mixer, pouring into the paste, and mixing with the paste. Such disturbances, especially during foam addition and mixing with the paste, liberated trapped gas and led to a foamed slurry with higher density and lower volume than expected (pure N₂ and CO₂/N₂: 1350 cm³, pure CO₂: 1440 cm³). The higher the CO₂ content was, the more gas was liberated and the lower the slurry volume was, owing to low preformed foam stability. For all samples, the slurry yield for pure N₂, 2:1 CO₂/N₂ gas mixture and, pure CO₂ was ~ 1250, 750, and 438 cm³, respectively. This led to an increase in the final FC density as more CO₂ was incorporated into the gas phase of the preformed foam.

The stability of the fresh foamed slurry as it sets is very crucial to ensure the uniformity of hardened FC pore structure and its properties. Fig. 4 shows that the addition of preformed foams based on CTAB either alone (Fig. 4a) or with lower content of CaCO₃ NPs (Fig. 4b and c) led to large pores separated with thin matrix at the top of the hardened cubes. This translates into a variation in density between the top and bottom sections of the FC cubes, and a clear indication of fresh slurry instability [5]. The stability of the bubbles within the fresh cement paste depends on the equilibrium state between the bubble confinement force resulting from the plastic density of the paste, drainage force relating to liquid film drainage under gravity, internal bubble pressure, surface tension, buoyancy force, and friction force [16,68]. Any reduction in surface tension or confinement force might lead to an increase in bubble size to approach equilibrium by reducing the internal bubble pressure [5]. Ostwald ripening might also occur within the foamed slurry due to the variation in bubble sizes causing large bubbles to become larger [16]. Once a certain size is reached, the buoyancy force becomes dominant and bubbles rise. The rising bubbles can reach the surface and burst or accumulate in layers displacing the paste, which causes instability and

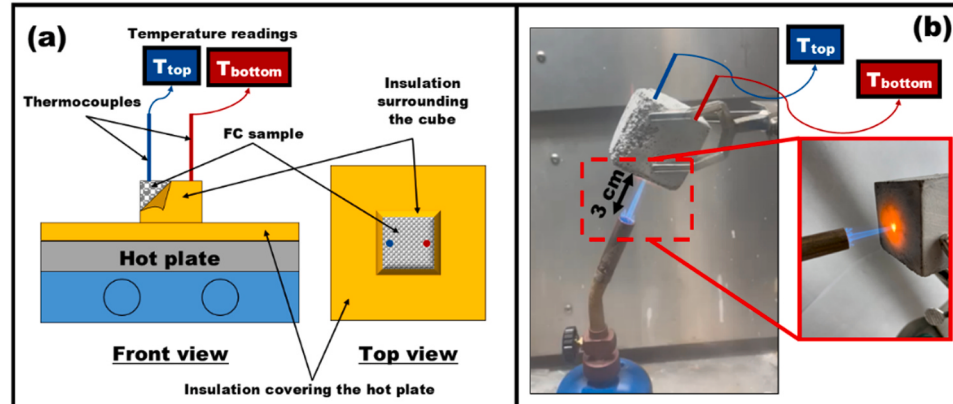


Fig. 2. Thermal insulation testing (a) for temperatures up to 90 °C and (b) under direct propane flame.

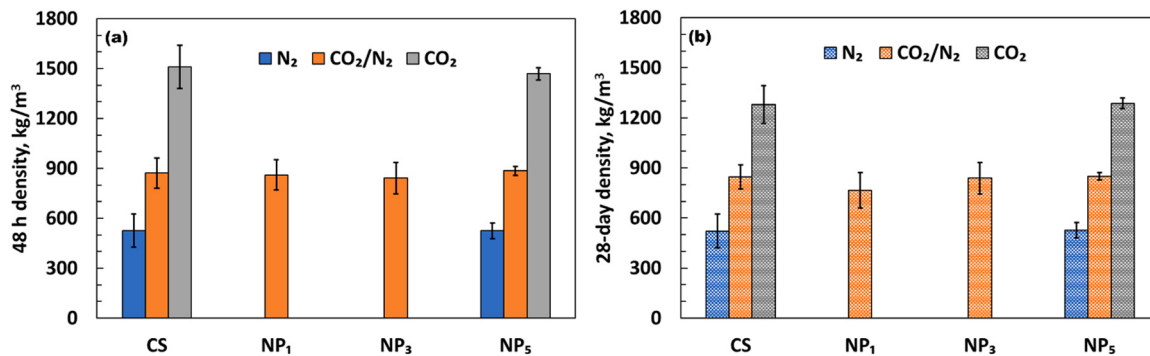


Fig. 3. FC density a) right after demolding (48 h) and b) at the end of the curing procedure (28 days).

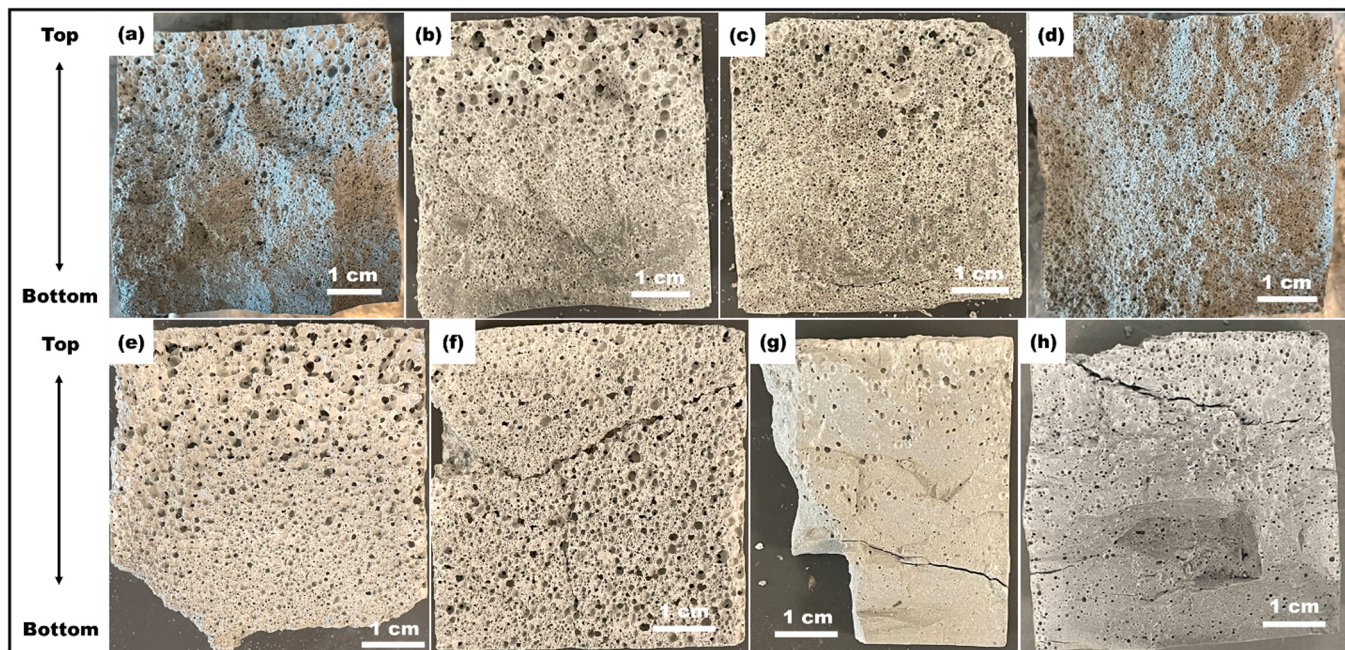


Fig. 4. Cross sectional images of FC made using a gas mixture of 2:1 CO₂/N₂ (a: CS, b: NP₁, c: NP₃ and d: NP₅), pure N₂ (e: CS and f: NP₅), and pure CO₂ (g: CS and h: NP₅). The images were taken after compressive strength testing.

uneven density distribution as can be seen in Fig. 4a–c, e and g. This process continues until equilibrium is established or the mix hardens [16]. At high NP content (NP₅), however, the pore structure looked more uniform (Fig. 4d, f and h). The initial small bubble size and high stability of NP₅ preformed foam [58] might have prevented the growth of the trapped bubbles to a size where they could become buoyant before the mix hardened. Moreover, the presence of high content of CaCO₃ NPs led to a more compact matrix around the pores which may have hindered gas diffusion as discussed below (Section 3.3). When compared to NP₅, the instability of CS, NP₁ and NP₃ led to a higher variation in the overall density of these samples as evident from the error bars in Fig. 3. It should be noted that the impact of instability was the worst in the case of FC made using CTAB foam with pure CO₂. The top of these FC cubes contained fragile layers (first 3–4 mm from the top) that got detached from the cubes during handling as seen in Figure S3. The image in Fig. 4g was taken after the removal of the fragile layer. This was not the case for FC made with CaCO₃ NPs/CTAB foam with pure CO₂.

Since samples made with pure CO₂ exhibited far less pore volume than the other gas phases, the upcoming discussion is largely focused on CS and NP₅ (most stable among all NP samples) made using pure N₂ and a 2:1 gas mixture of CO₂/N₂.

3.2. Compressive strength and water absorption of hardened FC

Compressive strength measurements after 28 days for FC produced from preformed foams with different gas phases are shown in Fig. 5. As expected, FC with higher densities showed higher compressive strengths. A compressive strength of 0.7 MPa was achieved for the FC made with pure N₂ regardless of the foaming solution/dispersion composition. The presence of CaCO₃ NPs did not seem to impact the strength, even though a more uniform pore structure was achieved for this FC. This could be due to the small amount of the matrix between the pores in these samples which overshadows any potential strength improvement. On the other hand, for a 2:1 CO₂/N₂ gas mixture, FC samples made from CaCO₃ NPs/CTAB foam (NP₅) had a 38% increase in their average compressive strength when compared to those from CTAB alone (CS). The presence of CaCO₃ NPs resulted in a more compact paste skeleton between the pores and less variation in pore sizes, to be discussed in Section 3.3, leading to higher and more consistent compressive strength measurements compared to FC without CaCO₃ NPs at the same density level. For FC produced from cement paste (initial w/c = 0.4) and protein-based preformed foam with similar curing process, Liu et al. [69] reported a compressive strength of around 0.5–1 and 2.5 MPa for FC densities between 500–600 and 800 kg/m³,

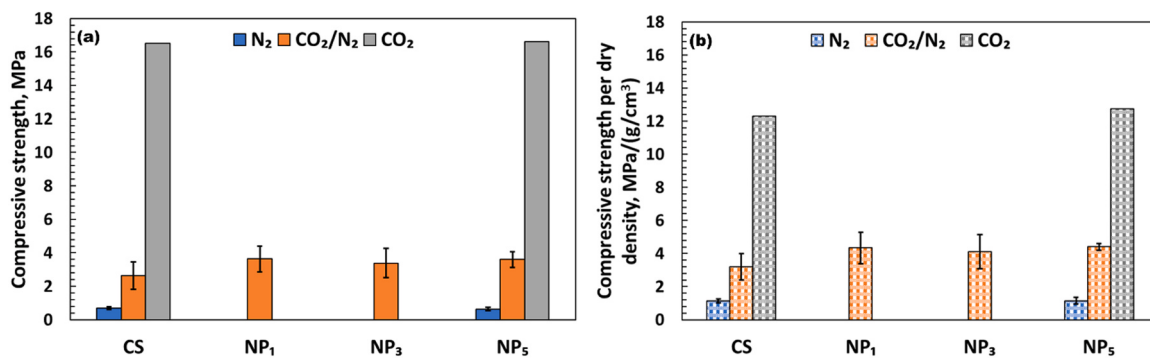


Fig. 5. 28-day compressive strength of FC samples made with N₂, CO₂ and CO₂/N₂ preformed foams in the presence and absence of CaCO₃ NPs. a) Absolute compressive strength (MPa) and b) normalized compressive strength (MPa/(g/cm³)).

respectively. The compressive strengths obtained in this study in the presence of CaCO₃ NPs (NP₅) were aligned with their [69] values at low densities (520 – 530 kg/m³) and showed improvements at higher densities (840 – 850 kg/m³). It is worth noting that compressive strengths reported in literature for FC vary significantly depending on several factors including binder material, dry density, filler material, porosity, foaming agent, w/c, production method, and curing process [12,19]. Chica and Alzate [12] and Amran et al. [13], in their reviews, reported values of 1 – 1.5 MPa (500 – 600 kg/m³), 1.5 – 3 MPa (800 – 1000 kg/m³), and 4.5 – 5.5 MPa (1200 kg/m³) whereas Tran et al. [3] cited values of 1 – 12 MPa (300–800 kg/m³) and 2 – 27 MPa (800 – 1200 kg/m³). FC made with nano-SiO₂ stabilized foams can achieve high compressive strengths likely due to their pozzolanic activity [5,10,33].

No significant change in compressive strength measurements was observed between CS and NP₅ FCs made with pure CO₂ foams (Fig. 5a). This, however, might not be a fair comparison due to the slurry instability of the CS samples. The strength value for NP₅ relates to a porous structure (Fig. 4h) whereas the value for CS is associated with a strength of a structure that is porous at the top and far less porous at the bottom (Fig. 4g). Since the cubes were tested on their side (Figure S2), the strength measurement for CS might be greatly influenced by the strength of the denser phase at the bottom as seen from the crack propagation in Fig. 4g. This argument also applies to CS samples made with pure N₂ and CO₂/N₂ mixture. Despite this unreliability, NP₅ still showed higher compressive strength than CS for the gas mixture.

Water absorption measurements after 24 h submersion are reported in Fig. 6. The lowest density cubes, the ones made using N₂ foams, showed the highest water absorption of ~ 30 vol%. With a 2:1 gas mixture CO₂/N₂, water absorption values were 15.3, 24.8, 18.0 and 14.9 vol% for CS, NP₁, NP₃ and NP₅, respectively. A reduction of 13% was observed between CS (17.4 vol%) and NP₅ (15.2 vol%) in the presence of pure CO₂. Water absorption of FC is not only related to the voids created by the foam bubbles, but also to the capillary (connected)

pores within the hydrated paste matrix [14,70]. The amount of paste present, composition of the paste, and w/c ratio all have an influence on water absorption via capillary suction [22]. The pure N₂ samples had lower density, more connected pores, and less compact hydrated paste between the pores than samples made with the gas mixture (Section r3.3); hence, it showed a higher water absorption. Even though less entrapped bubbles were visually observed in pure CO₂ samples (Fig. 4g and h) compared to the gas mixture, the higher overall w/c ratio might have led to an increase in capillary pores resulting in similar water absorption values. Similarly, CS had higher water absorption than NP₅ in the presence of pure CO₂ likely due to the higher w/c of CS compared to NP₅.

3.3. Microstructure and compositional analysis of hydrated FC

FC pore size distribution is presented in Fig. 7 from representative cross-sectional image analysis for the images in Fig. 8 as detailed in Section S4 of the supplementary material. FC from preformed foams made with CTAB foaming solution (CS) in the presence of pure N₂ (Fig. 7a) and a 2:1 CO₂/N₂ gas mixture (Fig. 7b) displayed variation in pore size distribution between the top and bottom of the cubes. This confirms the instability that was observed visually and discussed in Section r3.1. The instability and, thus, the variation in pore size distribution is more pronounced for FC made with pure N₂ (Fig. 7a) likely due to the lower overall density [16]. On the other hand, no significant variations in pore size distribution were observed between the top and bottom of FC samples made from 5 wt% CaCO₃/CTAB (NP₅) preformed foam (Fig. 7c and d). Furthermore, the initial small bubble sizes and higher stability of NP₅ preformed foam [58] led to an overall smaller pore sizes when compared to CS. For pure N₂ and a 2:1 CO₂/N₂ gas mixture, the maximum pore sizes detected for CS were 4.2 and 2.1 mm, respectively, while the maximum pore sizes for NP₅ were 1.7 and 1.1, respectively (Table 3). Even though the presence of CaCO₃ NPs resulted in a more homogeneous pore structure, larger pore sizes were observed at low density (pure N₂). Less cement paste existed between the bubbles (less confinement force) at low densities which allowed the bubbles to expand before the FC slurry hardened [16]. Moreover, pore connectivity was largely observed in samples with lower density such as pure N₂ samples (CS and NP₅) and top of CS made with CO₂/N₂ due to thin matrix separating the pores (Fig. 8). For the gas mixture, samples containing CaCO₃ NPs showed less pore connectivity than samples with CTAB alone. Hou et al. [24] observed more interconnected pores in FC made using CTAB than an anionic surfactant (sodium dodecyl sulfate). The positively charged CTAB molecules hinder the adsorption of the positively charged cement particles into the gas-liquid interface due to electrostatic repulsion creating a water-rich region around the pores [24]. Ions, such as Ca²⁺, SO₄²⁻ and AlO₂⁻, diffuse through the liquid layer and promote the formation of loose layers of portlandite and ettringite on the internal pore walls as evident by the SEM micrographs of Fig. 9

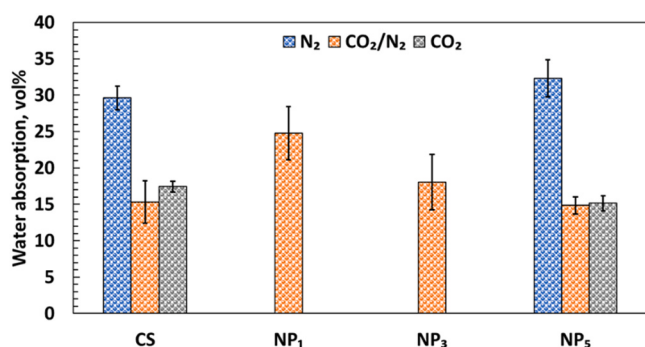


Fig. 6. Water absorption of FC samples after 24 h of being submerged in water.

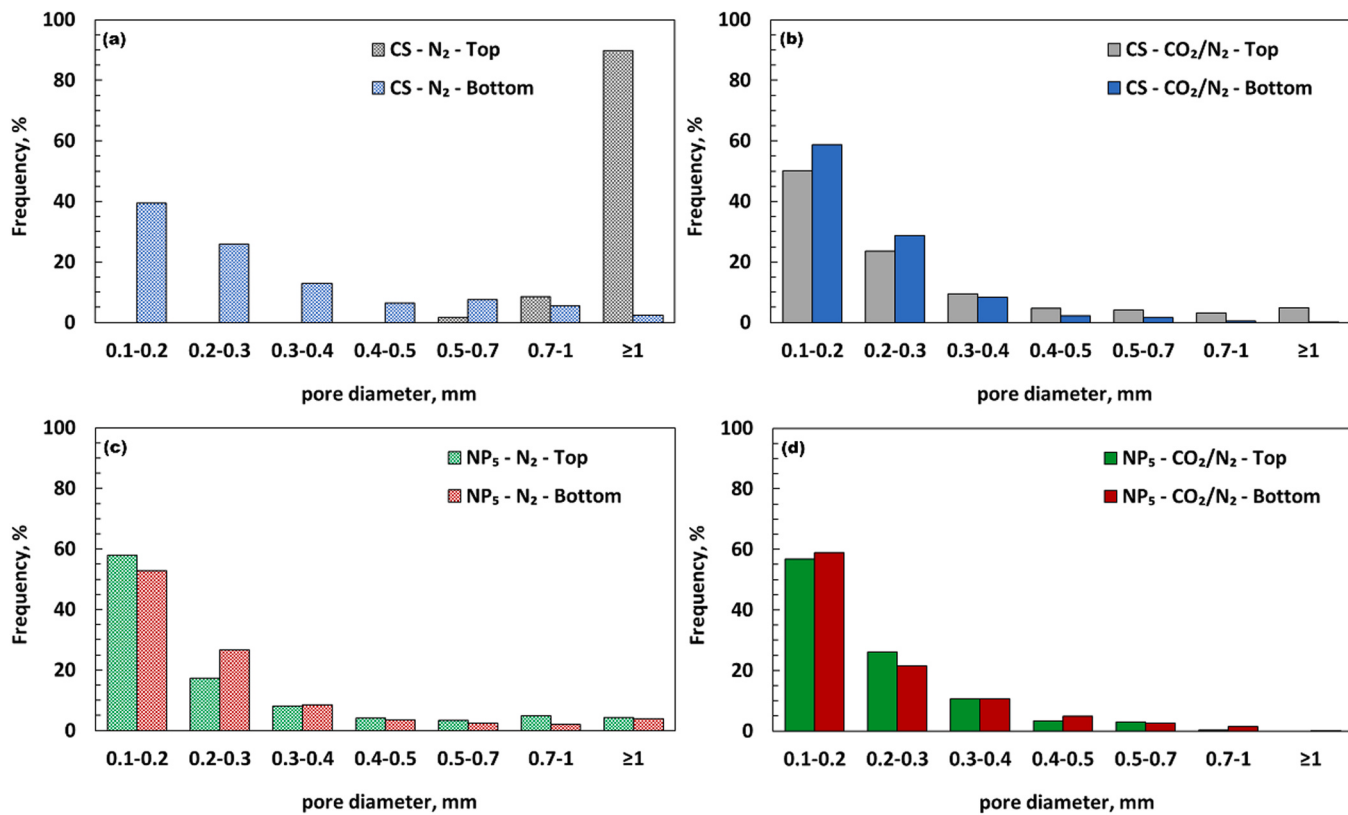


Fig. 7. Pore size distribution for: a and b) reference FC without CaCO₃ NPs (CS) made with N₂ alone and CO₂/N₂ mixture, respectively. c and d) FC with CaCO₃ NPs (NP₅) made with N₂ alone and CO₂/N₂ mixture, respectively.

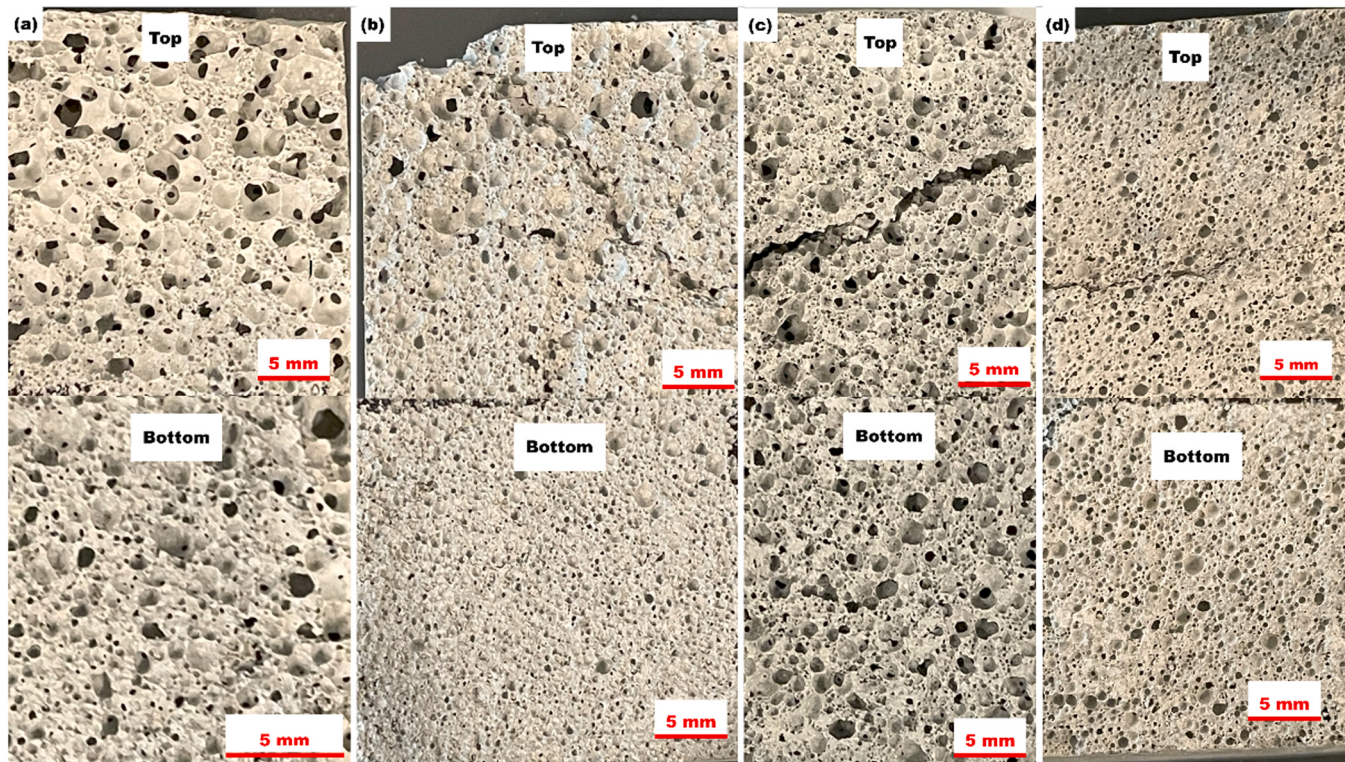


Fig. 8. Zoomed-in images from the top and bottom of FC cubes for a and b) reference FC without CaCO₃ NPs (CS) made with N₂ alone and CO₂/N₂ mixture, respectively. c and d) FC with CaCO₃ NPs (NP₅) made with N₂ alone and CO₂/N₂ mixture, respectively.

Table 3
Pore size distribution parameters.

Sample	Gas phase	Pore size parameters			
		Minimum, mm	Maximum, mm	Average, mm	Standard deviation, mm
CS	N ₂	0.11	4.2	0.41	0.48
	CO ₂ /N ₂ (2:1)	0.11	2.1	0.25	0.21
NP ₅	N ₂	0.11	1.7	0.28	0.26
	CO ₂ /N ₂ (2:1)	0.10	1.1	0.22	0.12

and Fig. 10.

SEM micrographs of CS and NP₅ FCs produced using pure N₂ and a 2:1 gas mixture of CO₂/N₂ are shown in Fig. 9 and Fig. 10, respectively. The microstructure of the top (Fig. 9a–c) of the CS cube made using pure N₂ was different than that of the bottom (Fig. 9d,e). Two types of pore morphologies were observed at the top of the CS cube. Larger connected pores (> 0.8 mm) were lined with clusters of CaCO₃ (calcite) crystals (Fig. 9a) formed due to the carbonation reactions with CO₂ from the atmosphere, whereas smaller pores mostly contained needle-like ettringite (3CaO·Al₂O₃·3CaSO₄·32 H₂O) along with some prismatic portlandite (Ca(OH)₂) crystals (Fig. 9b) as confirmed by EDX. The EDX analysis of the hydrated paste between the pores indicated the presence of areas with rich calcium-silicate-hydrate (C-S-H) phases (Ca/Si ~ 1.5 – 2) and other areas with CaCO₃ crystals (Fig. 9c). The bottom part of CS – N₂, however, showed flaky portlandite and needle-like ettringite covering the inside of the pores (Fig. 9d) and C-S-H phases between the pores

(Fig. 9e). The rise of buoyant gas bubbles within the CS – N₂ slurry led to phase separation where cement paste was forced to the bottom of the cube creating a denser phase of hydration products and less connected pores that reduced atmospheric carbonation. Therefore, more calcite and traces of portlandite were detected at the top whereas more portlandite and less calcite existed at the bottom for CS – N₂ as confirmed by both TGA (Fig. 11a and Table 4) and XRD (Fig. 12a) analysis. The utilization of CaCO₃ NP-stabilized N₂ foam (NP₅ – N₂) led to more uniformity in the microstructure between the top and the bottom of the cubes. Larger pores contained a layer of CaCO₃ underneath portlandite flakes and ettringite (Fig. 9g) while smaller pores were covered by only flaky portlandite and needle-like ettringite (Fig. 9h). The hydrated matrix between the pores (Fig. 9i) was rich in C-S-H phases and portlandite crystals and looked more compact than that of the top of CS – N₂ (Fig. 9c) preventing excessive atmospheric carbonation. These observations also apply to the bottom of NP₅ – N₂.

FC generated with a 2:1 CO₂/N₂ foam had more cement paste around the pores due to the higher density (Section 3.1). The top and the bottom of CS – CO₂/N₂ and NP₅ - CO₂/N₂ samples showed portlandite and ettringite on the internal pore walls (Fig. 10a,f). However, large pores (>0.9 mm) in the top section of CS – CO₂/N₂ were not lined completely with portlandite and ettringite. A layer of C-S-H could be seen in the spaces that were not occupied by either portlandite or ettringite (Fig. 10b). Smaller pores in the top section of CS – CO₂/N₂ and the pores in the bottom section of CS – CO₂/N₂ along with the pores in the top and the bottom sections of NP₅ - CO₂/N₂ showed compact portlandite and ettringite layers covering the internal pore structures, similar to Fig. 10c. Furthermore, some of the pores at the top section of NP₅ - CO₂/N₂ had CaCO₃ crystals formed on top of the flaky portlandite

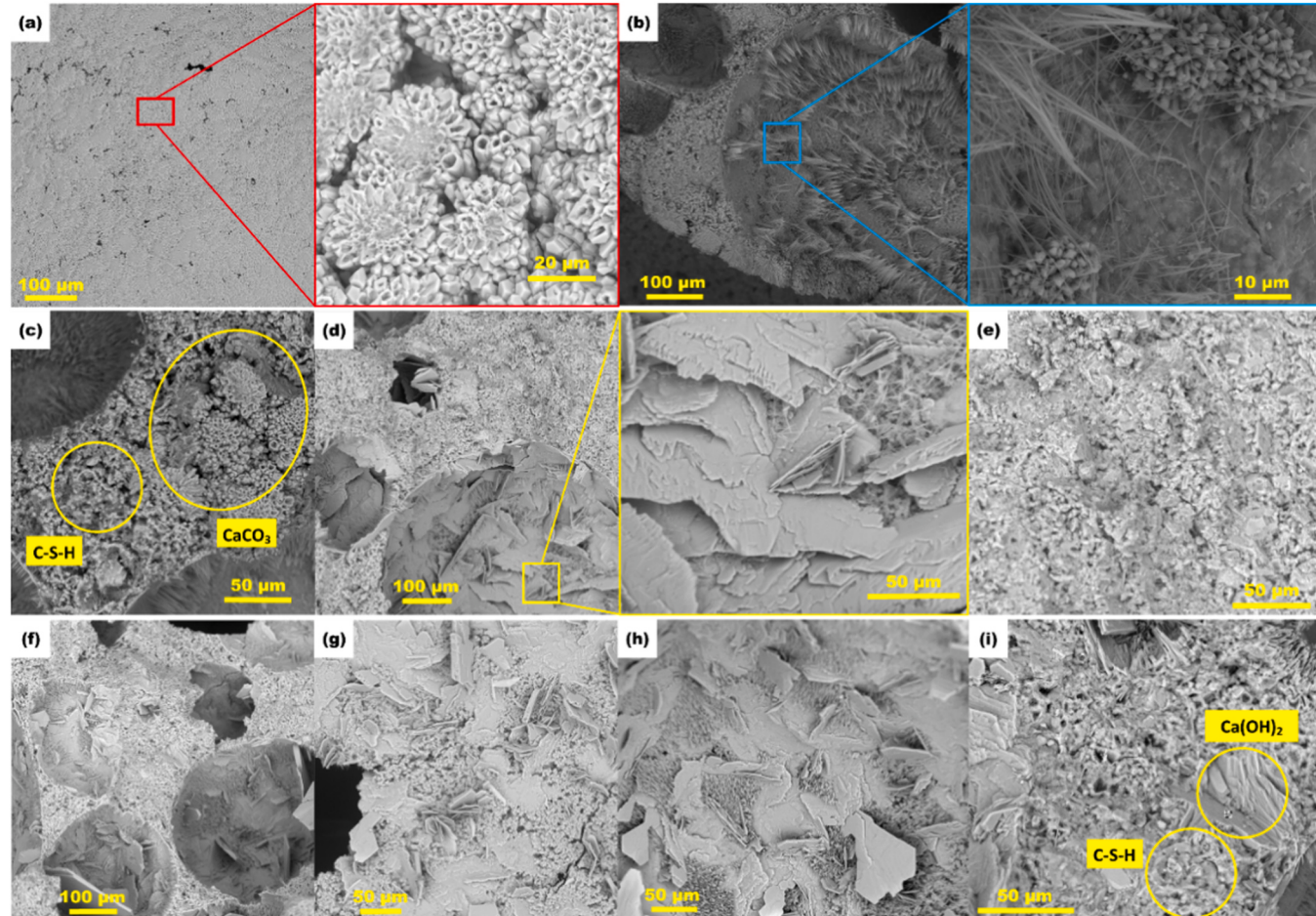


Fig. 9. SEM micrographs for the top (a – c) and bottom (d and e) of a CS cube and the top (f – i) of NP₅ cube made using pure N₂ foam.

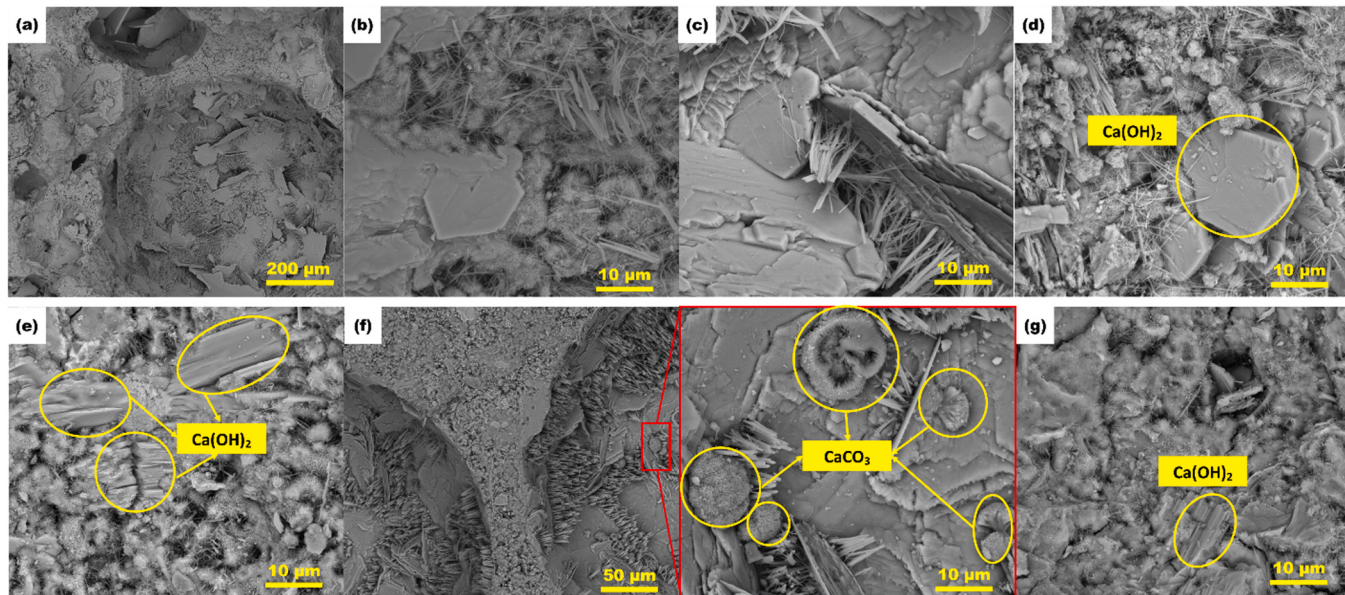


Fig. 10. SEM micrographs for the top (a – d) and bottom (e) of a CS cube and the top (f and g) of a NP₅ cube made using CO₂/N₂ foam.

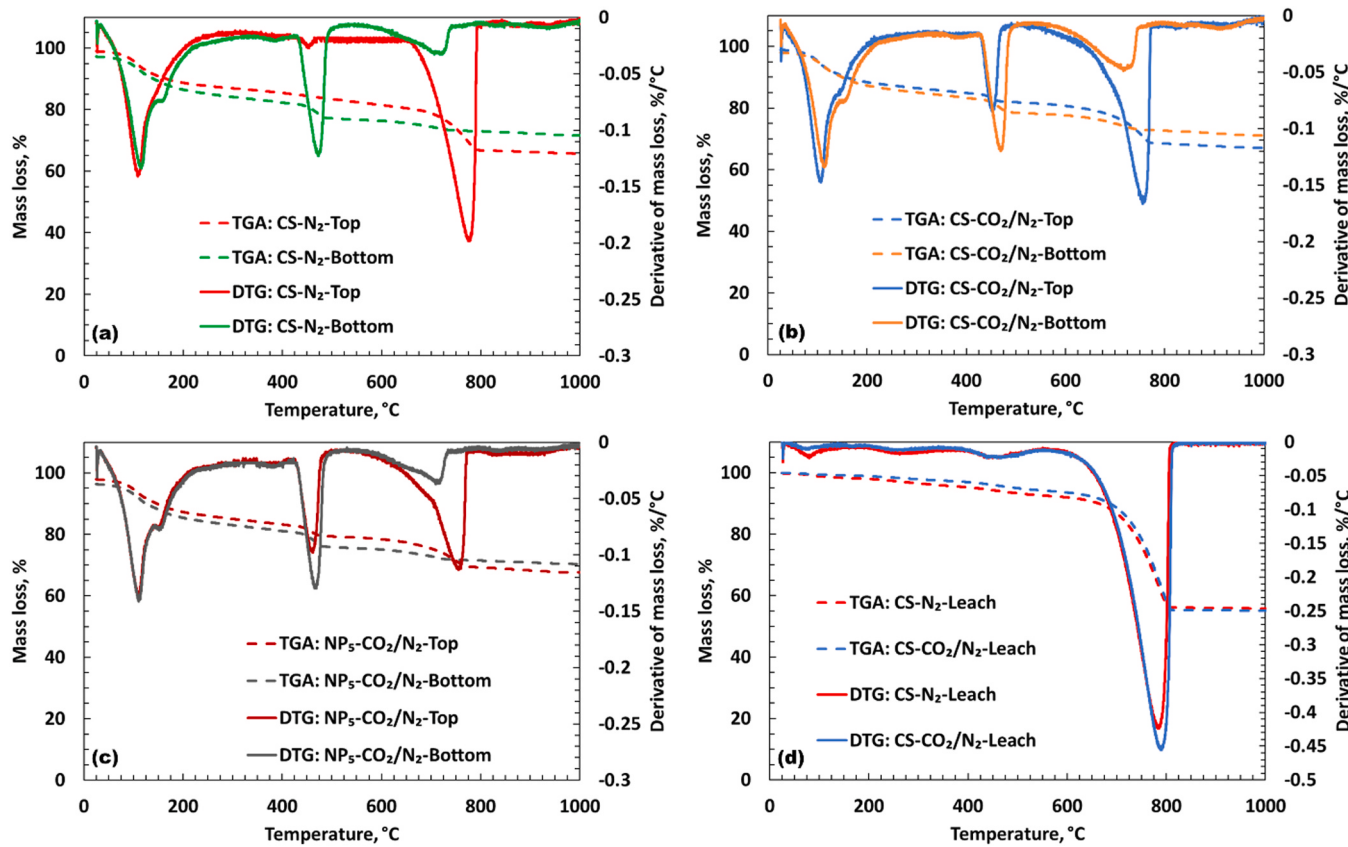


Fig. 11. TGA and DTG curves for the top and bottom of CS cubes in the presence of N₂ alone (a) and CO₂/N₂ mixture (b), the top and bottom of NP₅ cubes in the presence of CO₂/N₂ gas mixture (c), and the leached material covering the surface of CS cubes (d).

crystals (Fig. 10f). This carbonation might be from the CO₂ either trapped within the foam or diffused from the atmosphere. Even though the morphology of the crystals was unusual for calcite, the XRD patterns presented in Fig. 12 identifies calcite as the only CaCO₃ polymorph detected in all the samples. The presence of CTAB at the gas-liquid interface might have impacted the morphology of the hydration and carbonation products. Moreover, since the added CaCO₃ NPs were

hydrophilic and did not adsorb at the gas-liquid interface [58], these NPs likely became part of the hydrated paste between the pores. The presence of CaCO₃ NPs within the hydrated matrix promoted further hydration of Portland cement and reduced its induction period as can be inferred from intensity and shift of the heat flow peaks in Fig. 13a as well as the higher cumulative heat in Fig. 13b compared to samples with CTAB alone. CaCO₃ NPs can act as nucleation sites promoting the

Table 4

Estimated $\text{Ca}(\text{OH})_2$ (400 – 500 °C) and CaCO_3 (500 – 800 °C) content (wt% of the hydrated paste) from TGA mass loss.

Sample	Position within sample	$\text{Ca}(\text{OH})_2$, wt%	CaCO_3 , wt%
CS – N ₂	Top	1.0	22.0
	Bottom	15.4	3.8
CS – CO ₂ /N ₂	Top	7.2	20.4
	Bottom	15.4	6.7
NP ₅ – CO ₂ /N ₂	Top	10.9	13.4
	Bottom	16.0	4.0

formation of C-S-H gel and portlandite crystals [51,71]. As a result, a more compact hydrated matrix and smaller portlandite crystals were observed between the pores in NP₅ (Fig. 10g) when compared to that of

CS (Fig. 10d,e). The XRD pattern of NP₅ – CO₂/N₂ also indicated traces of hemi- and monocarboaluminates (Fig. 12c), which were not detected in samples without CaCO₃ NPs (Fig. 12a,b). Therefore, the CaCO₃ NPs promoted the formation of carboaluminate phases such as calcium hemi- and monocarboaluminates in the cement paste, as also reported in the literature [15,71,72].

The TGA and derivative thermogravimetry (DTG) curves (Fig. 11a–c) showed variation in the amount of CaCO₃ between the top and bottom of CS and NP₅ samples made using pure N₂ and a mixture of CO₂/N₂. Although CaCO₃/CTAB (NP₅) foam made from a CO₂/N₂ (2:1) gas mixture was far more stable than CTAB alone (CS) [58], the NP₅ – CO₂/N₂ sample showed the least CaCO₃ mass loss (Table 4). In fact, CS in the absence of CO₂ (CS – N₂) had the highest carbonation level at the top. For all samples, there was more carbonation at the top than the

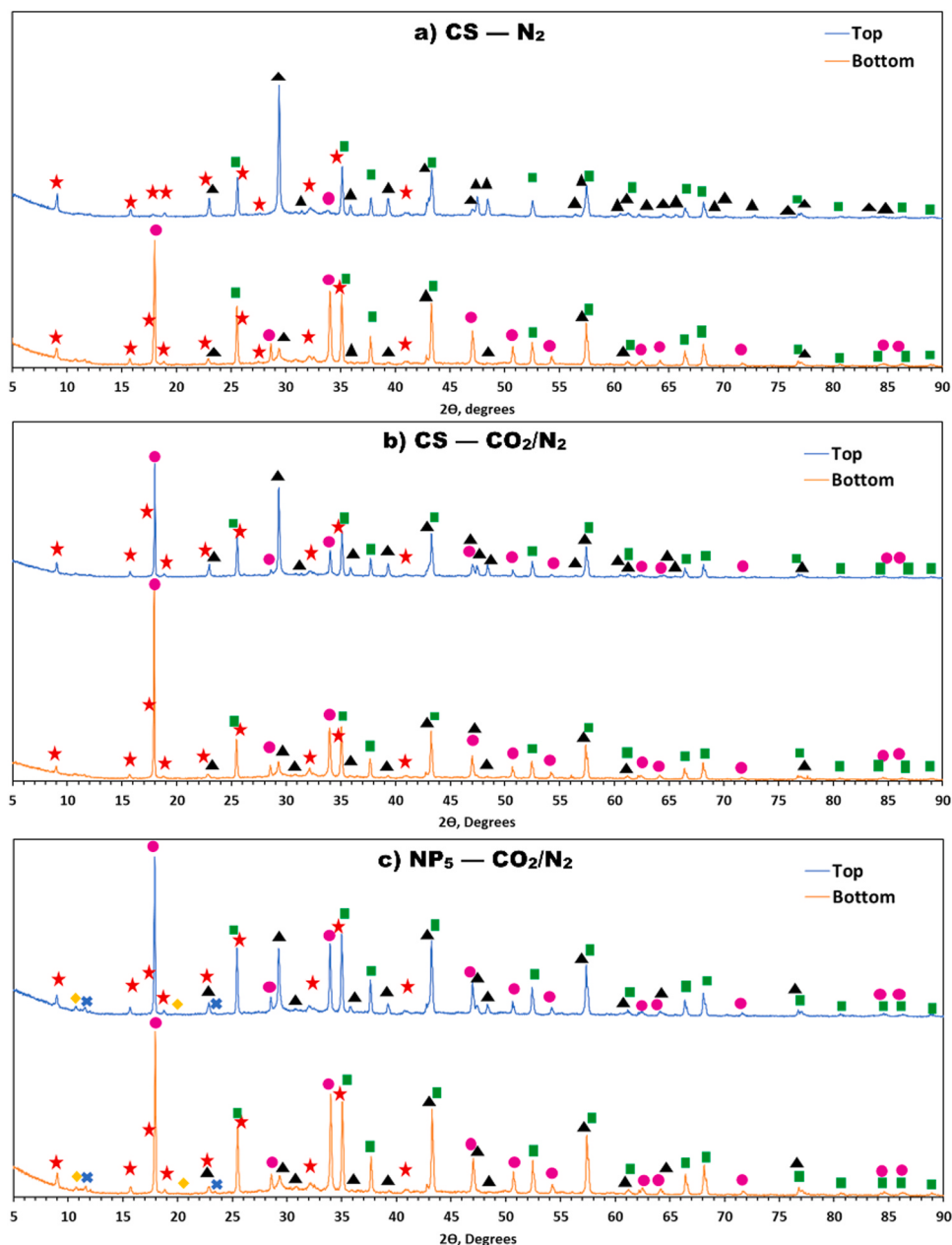


Fig. 12. XRD patterns for ground FC samples taken from the top and bottom of CS and NP₅ cubes showing reflections for ettringite (★), calcite (▲), portlandite (●), hemicarboaluminate (◆), monocarboaluminate (×), and corundum (■).

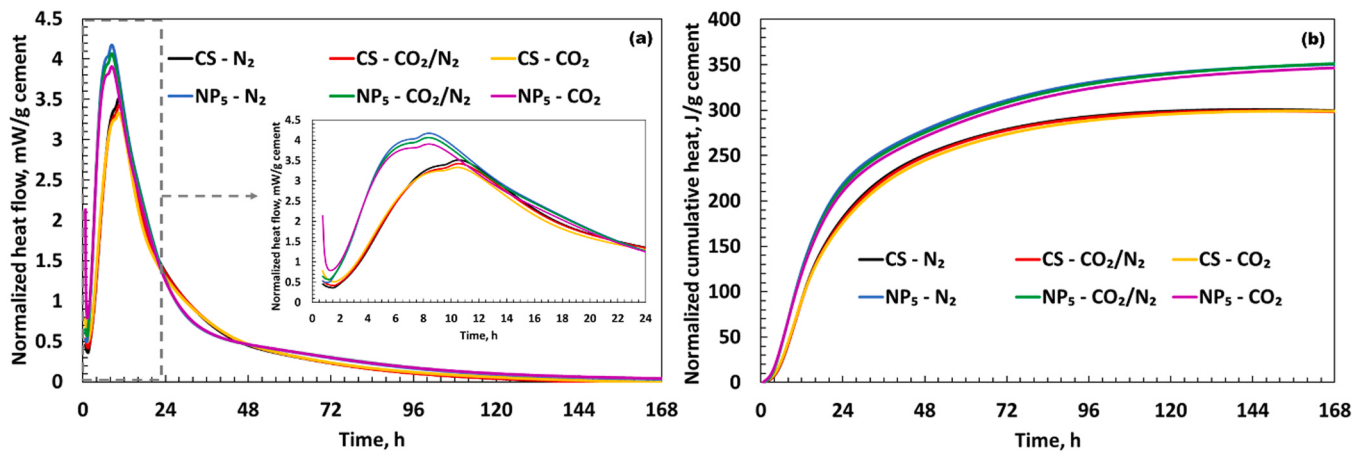


Fig. 13. Heat evolution (a) and cumulative heat (b) of cement pastes (w/c of 0.6) made with 0.05 wt% CTAB solution (CS) and 5 wt% CaCO₃ NPs/0.05 wt% CTAB dispersion (NP₅) in the presence of different gas phases at 25 °C.

bottom due to the reaction of portlandite, and possibly other hydrate-d/anhydrous phases, with atmospheric CO₂. This makes it difficult to estimate the amount of CO₂ captured, if any, from the CO₂/N₂ preformed foams. The denser matrix in the presence of CaCO₃ NPs reduced the carbonation level, as can be seen in Table 4.

It is worth noting that the outside surfaces of some CS samples (all gas phases) were covered with Ca(OH)₂ and CaCO₃, according to TGA and DTG (Fig. 11d), during the curing process indicating leaching. This was also observed in NP₅ made with pure N₂, however, not in NP₅ made with the gas mixture most likely due to low pore connectivity.

3.4. Thermal insulation of FC

The surface temperatures of CS and NP₅ cubes constructed using pure N₂ and CO₂/N₂ preformed foam after 60 min of heating at different heating plate temperatures are reported in Fig. 14a. The instability in the CS samples was very clear as the top and bottom of the cubes transferred heat at different rates, causing variation of surface temperature. This variation was amplified with increasing the hot plate temperature. The NP₅ samples, however, showed more uniform surface temperatures between the top and the bottom of the cubes. NP₅ made using pure N₂ (NP₅ - N₂) had better heat transfer resistance than that made of CO₂/N₂ foam (NP₅ - CO₂/N₂) due to the lower density. The lower FC density translates to more gas voids. Since heat convection can be neglected in small voids, heat transfer through FC is dominated by heat conduction via the hydrated cement paste skeleton and the gas inside the voids [10].

Accordingly, low FC thermal conductivity is expected for high porosity FC due to the significantly lower thermal conductivity of the gas compared to that of the hydrated paste. This is evident from the lower thermal resistance of regular cement paste (no foam added) compared to the FC samples in Fig. 14a. Furthermore, the estimated thermal conductivity (Section S5 of the supplementary material) was around 0.14 and 0.15 W/m.K for NP₅ - N₂ (~530 kg/m³) and NP₅ - CO₂/N₂ (~850 kg/m³), respectively. These values are lower than the ones reported by Du et. al. [10] (0.1 – 0.2 W/m.K for 400 – 600 kg/m³ and 0.26 – 0.37 W/m.K for 800 – 1000 kg/m³) for FC made from modified nano-SiO₂ and hydroxypropyl methylcellulose stabilized foam. The reported values in this study also fall in the lower end of the ranges cited by Chica and Alzate [12] and Amran et al. [13] in their reviews (0.08 – 0.17 W/m.K for 500 – 600 kg/m³ and 0.17 – 0.3 W/m.K for 800 – 1000 kg/m³).

When exposed to a propane flame (T > 1000 °C) for 5 min, all FC samples maintained their structure after burning. There were surface cracks that developed across the surface exposed to the flame (Figures S5 and S6), however, they did not penetrate deep into the structure. The highest recorded temperature during the burning process on the surface opposite to the surface exposed to the flame is shown in Fig. 14b. The FC with CaCO₃ NPs/CTAB (NP₅) demonstrated higher thermal resistance than FC with CTAB alone (CS), most likely due to the uniformity of the NP₅ pore structure.

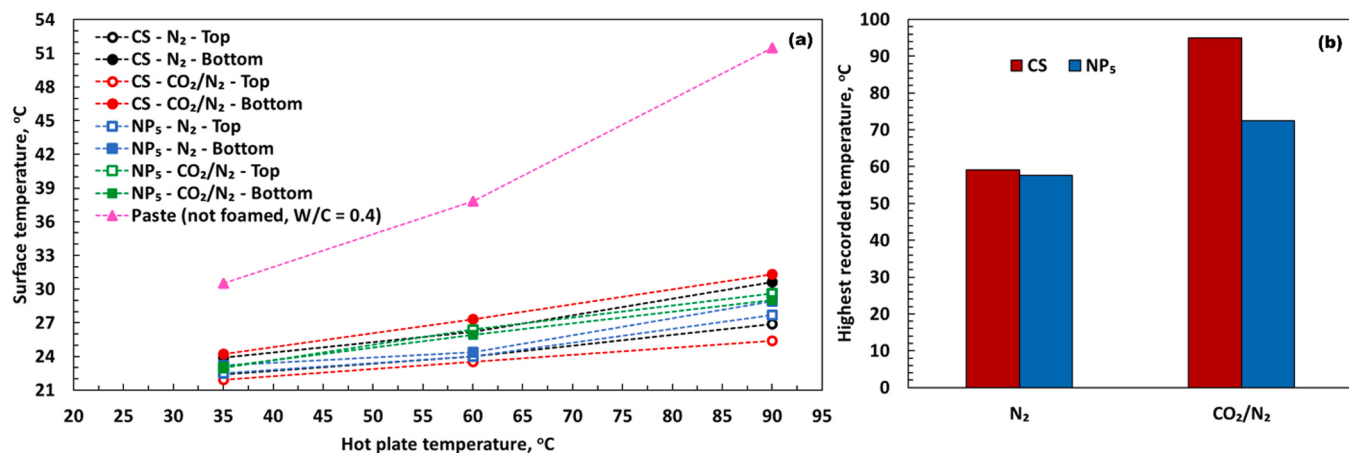


Fig. 14. (a) cube surface temperature after 60 min of heating at different heating plate temperatures and (b) highest recorded temperature on the cube surface that is opposite to the surface exposed to a propane flame after 5 min of burning.

4. Conclusions

The stability of the FC slurry as it sets is very crucial to achieve homogenous properties within the FC. In this study, the use of CaCO_3 NPs/CTAB stabilized preformed foams stabilized the FC slurry and led to a more uniform and narrower pore size distribution compared to foams with CTAB alone. The high stability and smaller bubble sizes of CaCO_3 NPs/CTAB foam maintained sufficiently small bubbles to resist buoyance within the FC slurry. Furthermore, the dry density of FC increased with increasing the CO_2 content of the gas phase due to gas escape. The compressive strength of all FC samples increased with increasing density while their water absorption decreased. The instability of FC made using CTAB foam, especially for pure N_2 , caused significant atmospheric carbonation particularly at the top of the samples. Alternatively, the CaCO_3 NPs acted as nucleation sites for C-S-H within the solid skeleton surrounding the pores resulting in a C-S-H rich and denser matrix. This led to improvement in compressive strength, less connected pore structure, and reduced atmospheric carbonation. Lastly, the higher FC stability in the presence of CaCO_3 NPs enhanced the thermal insulation performance of FC.

CRediT authorship contribution statement

Ahmed G. Mehairi: Conceptualization, Data curation, Formal analysis, Investigation, Methodology, Resources, Validation, Visualization, Writing – original draft, Writing – review & editing. **Rahil Khoshnazar:** Conceptualization, Funding acquisition, Investigation, Methodology, Project administration, Resources, Supervision, Validation, Writing – review & editing. **Maen M. Husein:** Conceptualization, Funding acquisition, Investigation, Methodology, Project administration, Resources, Supervision, Validation, Writing – review & editing.

Declaration of Competing Interest

The authors declare that they have no known competing financial interests or personal relationships that could have appeared to influence the work reported in this paper.

Data Availability

Data will be made available on request.

Acknowledgements

The authors would like to acknowledge the financial support of NSERC Discovery grants (Grant number: RGPIN-2020-03880 and RGPIN-2018-04755).

Appendix A. Supporting information

Supplementary data associated with this article can be found in the online version at [doi:10.1016/j.conbuildmat.2024.135927](https://doi.org/10.1016/j.conbuildmat.2024.135927).

References

- [1] A. Gadkar, K.V.L. Subramaniam, Tailoring porosity and pore structure of cellular geopolymers for strength and thermal conductivity, Constr. Build. Mater. 393 (2023) 132150, <https://doi.org/10.1016/j.conbuildmat.2023.132150>.
- [2] J. Dang, S. Zhao, G. Chen, X. Cao, J. Yang, Effect of polyethylene powder and heating treatment on the microstructure and hardened properties of foam concrete, J. Build. Eng. 50 (2022) 104143, <https://doi.org/10.1016/j.jobe.2022.104143>.
- [3] N.P. Tran, T.N. Nguyen, T.D. Ngo, P.K. Le, T.A. Le, Strategic progress in foam stabilisation towards high-performance foam concrete for building sustainability: a state-of-the-art review, J. Clean. Prod. 375 (2022) 133939, <https://doi.org/10.1016/j.jclepro.2022.133939>.
- [4] Z. Pan, H. Li, W. Liu, Preparation and characterization of super low density foamed concrete from Portland cement and admixtures, Constr. Build. Mater. 72 (2014) 256–261, <https://doi.org/10.1016/j.conbuildmat.2014.08.078>.
- [5] W. She, Y. Du, C. Miao, J. Liu, G. Zhao, J. Jiang, Y. Zhang, Application of organic- and nanoparticle-modified foams in foamed concrete: reinforcement and stabilization mechanisms, Cem. Concr. Res. 106 (2018) 12–22, <https://doi.org/10.1016/j.cemconres.2018.01.020>.
- [6] B. Meskhi, A.N. Beskopylny, S.A. Stel'makh, E.M. Shcherban', L.R. Mailyan, N. Beskopylny, A. Chernil'nik, D. El'shaeva, Insulation foam concrete nanomodified with microsilica and reinforced with polypropylene fiber for the improvement of characteristics, Polym. (Basel) 14 (2022) 4401, <https://doi.org/10.3390/polym14204401>.
- [7] Y.H.M. Amran, N. Farzadnia, A.A.A. Ali, Properties and applications of foamed concrete; a review, Constr. Build. Mater. 101 (2015) 990–1005, <https://doi.org/10.1016/j.conbuildmat.2015.10.112>.
- [8] X. Wang, J. Huang, S. Dai, B. Ma, Q. Jiang, Investigation of silica fume as foam cell stabilizer for foamed concrete, Constr. Build. Mater. 237 (2020) 117514, <https://doi.org/10.1016/j.conbuildmat.2019.117514>.
- [9] R. Kou, M.Z. Guo, Y. Shi, M. Mei, L. Jiang, H. Chu, Y. Zhang, H. Shen, L. Xue, Sound-insulation and photocatalytic foamed concrete prepared with dredged sediment, J. Clean. Prod. 356 (2022) 131902, <https://doi.org/10.1016/j.jclepro.2022.131902>.
- [10] Z. Du, W. Zuo, P. Wang, W. She, Ultralight, super thermal insulation, and fire-resistant cellular cement fabricated with Janus nanoparticle stabilized ultra-stable aqueous foam, Cem. Concr. Res. 162 (2022) 106994, <https://doi.org/10.1016/j.cemconres.2022.106994>.
- [11] M. Abd Elrahman, P. Sikora, S.Y. Chung, D. Stephan, The performance of ultralightweight foamed concrete incorporating nanosilica, Arch. Civ. Mech. Eng. 21 (2021) 79, <https://doi.org/10.1007/s43452-021-00234-2>.
- [12] L. Chica, A. Alzate, Cellular concrete review: new trends for application in construction, Constr. Build. Mater. 200 (2019) 637–647, <https://doi.org/10.1016/j.conbuildmat.2018.12.136>.
- [13] M. Amran, A.M. Onaizi, R. Fediuk, A. Danish, N.I. Vatin, G. Murali, H. S. Abdelgader, M.A. Mosaberpanah, D. Cecchin, A. Azevedo, An ultra-lightweight cellular concrete for geotechnical applications – a review, Case Stud. Constr. Mater. 16 (2022) e01096, <https://doi.org/10.1016/j.cscm.2022.e01096>.
- [14] Y. Xiong, Y. Zhu, C. Chen, Y. Zhang, Effect of nano-alumina modified foaming agents on properties of foamed concrete, Constr. Build. Mater. 267 (2021) 121045, <https://doi.org/10.1016/j.conbuildmat.2020.121045>.
- [15] M.A.O. Mydin, P. Jagadesh, A. Bahrami, A. Dulaimi, Y.O. Özkiç, M.M. Al Bakri Abdullah, R.P. Jaya, Use of calcium carbonate nanoparticles in production of nano-engineered foamed concrete, J. Mater. Res. Technol. 26 (2023) 4405–4422, <https://doi.org/10.1016/j.jmrt.2023.08.106>.
- [16] M.R. Jones, L. Zheng, K. Ozlutas, Stability and instability of foamed concrete, Mag. Concr. Res. 68 (2016) 542–549, <https://doi.org/10.1680/macr.15.00097>.
- [17] K. Ramamurthy, E.K. Kunhanandan Nambiar, G. Indu Siva Ranjani, A classification of studies on properties of foam concrete, Cem. Concr. Compos. 31 (2009) 388–396, <https://doi.org/10.1016/j.cemconcomp.2009.04.006>.
- [18] K. Dhasindrakrishna, S. Ramakrishnan, K. Pasupathy, J. Sanjay, Collapse of fresh foam concrete: mechanisms and influencing parameters, Cem. Concr. Compos. 122 (2021) 104151, <https://doi.org/10.1016/j.cemconcomp.2021.104151>.
- [19] O. Gencel, T. Bilir, Z. Bademler, T. Ozbakkaloglu, A detailed review on foam concrete composites: ingredients, properties, and microstructure, Appl. Sci. 12 (2022) 5752, <https://doi.org/10.3390/app12115752>.
- [20] A. Raj, D. Sathyan, K.M. Mini, Physical and functional characteristics of foam concrete: a review, Constr. Build. Mater. 221 (2019) 787–799, <https://doi.org/10.1016/j.conbuildmat.2019.06.052>.
- [21] M. Amran, R. Fediuk, N. Vatin, Y.H. Lee, G. Murali, T. Ozbakkaloglu, S. Klyuev, H. Alabduljabber, Fibre-reinforced foamed concretes: a review, Mater. (Basel) 13 (2020) 4323, <https://doi.org/10.3390/ma13194323>.
- [22] R. Othman, R. Putra Jaya, Y. Duraisamy, M.A. Sulaiman, B.W. Chong, A. Ghamari, Efficiency of waste as cement replacement in foamed concrete—a review, Sustainability 15 (2023) 5163, <https://doi.org/10.3390/su15065163>.
- [23] T.T. Nguyen, H.H. Bui, T.D. Ngo, G.D. Nguyen, Experimental and numerical investigation of influence of air-voids on the compressive behaviour of foamed concrete, Mater. Des. 130 (2017) 103–119, <https://doi.org/10.1016/j.matdes.2017.05.054>.
- [24] L. Hou, J. Li, Z. Lu, Y. Niu, Influence of foaming agent on cement and foam concrete, Constr. Build. Mater. 280 (2021) 122399, <https://doi.org/10.1016/j.conbuildmat.2021.122399>.
- [25] A. Just, B. Middendorf, Microstructure of high-strength foam concrete, Mater. Charact. 60 (2009) 741–748, <https://doi.org/10.1016/j.matchar.2008.12.011>.
- [26] W. She, Z. Zheng, Q. Zhang, W. Zuo, J. Yang, Y. Zhang, L. Zheng, J. Hong, C. Miao, Predesigning matrix-directed super-hydrophobization and hierarchical strengthening of cement foam, Cem. Concr. Res. 131 (2020) 106029, <https://doi.org/10.1016/j.cemconres.2020.106029>.
- [27] B. Mazian, E. Wirquin, K. Agubbi, P. Martin, L. Chaveriat, V. Dubois, Effect of mixing conditions on the density, morphology, thermal and mechanical properties of mineral foam, J. Build. Eng. 52 (2022) 104410, <https://doi.org/10.1016/j.jobc.2022.104410>.
- [28] C. Sun, Y. Zhu, J. Guo, Y. Zhang, G. Sun, Effects of foaming agent type on the workability, drying shrinkage, frost resistance and pore distribution of foamed concrete, Constr. Build. Mater. 186 (2018) 833–839, <https://doi.org/10.1016/j.conbuildmat.2018.08.019>.
- [29] Y. Fu, X. Wang, L. Wang, Y. Li, Foam concrete: a state-of-the-art and state-of-the-practice review, Adv. Mater. Sci. Eng. 2020 (2020) 1–25, <https://doi.org/10.1155/2020/6153602>.
- [30] Z. Du, J. Xiong, W. Zuo, W. She, Using modified nano-silica to prevent bubble Ostwald ripening under low atmospheric pressure: from liquid foam to air-

- entrained cement mortar, *Cem. Concr. Compos.* 132 (2022) 104627, <https://doi.org/10.1016/j.cemconcomp.2022.104627>.
- [31] Y. Zhang, Q. Liu, H. Ye, L.L. Yang, D. Luo, B. Peng, Nanoparticles as foam stabilizer: Mechanism, control parameters and application in foam flooding for enhanced oil recovery, *J. Pet. Sci. Eng.* 202 (2021) 108561, <https://doi.org/10.1016/j.petrol.2021.108561>.
- [32] M. Issakhov, M. Shakeel, P. Pourafshary, S. Aidarova, A. Sharipova, Hybrid surfactant-nanoparticles assisted CO₂ foam flooding for improved foam stability: a review of principles and applications, *Pet. Res.* 7 (2022) 186–203, <https://doi.org/10.1016/j.ptlrs.2021.10.004>.
- [33] L. Hou, J. Li, Z. Lu, Y. Niu, J. Jiang, T. Li, Effect of nanoparticles on foaming agent and the foamed concrete, *Constr. Build. Mater.* 227 (2019) 116698, <https://doi.org/10.1016/j.conbuildmat.2019.116698>.
- [34] A. Sychova, M. Sychov, E. Rusanova, A method of obtaining geoinseprotective foam concrete for use on railway transport, *Procedia Eng.* 189 (2017) 681–687, <https://doi.org/10.1016/j.proeng.2017.05.108>.
- [35] J. Gong, L. Zhu, J. Li, D. Shi, Silica fume and nanosilica effects on mechanical and shrinkage properties of foam concrete for structural application, *Adv. Mater. Sci. Eng.* 2020 (2020) 1–10, <https://doi.org/10.1155/2020/3963089>.
- [36] T. Sivakumar, B. Bhuvaneshwari, P. Prabha, R. Regupathi, Characteristics of functionally modified foamed concrete by nano-silica, *Int. J. Eng. Res. Technol.* 3 (2014) 1447–1452.
- [37] H. Jia, B. Cui, G. Niu, J. Chen, Y. Yang, Q. Wang, C. Tang, Experimental and mechanism study on the impermeability and thermal insulation of foam concrete regulated by nano-silica and fluorine-free foam, *J. Build. Eng.* 64 (2023) 105675, <https://doi.org/10.1016/j.jobe.2022.105675>.
- [38] C. Krämer, M. Schauer, T.L. Kowald, R.H.F. Trettin, Three-phase-foams for foam concrete application, *Mater. Charact.* 102 (2015) 173–179, <https://doi.org/10.1016/j.matchar.2015.03.004>.
- [39] C. Krämer, M. Schauer, T. Müller, S. Gebhard, R. Trettin, Application of reinforced three-phase-foams in UHPC foam concrete, *Constr. Build. Mater.* 131 (2017) 746–757, <https://doi.org/10.1016/j.conbuildmat.2016.11.027>.
- [40] X. Yuanliang, L. Baoliang, C. Chun, Z. Yamei, Properties of foamed concrete with Ca(OH)₂ as foam stabilizer, *Cem. Concr. Compos.* 118 (2021) 103985, <https://doi.org/10.1016/j.cemconcomp.2021.103985>.
- [41] S. Guo, W. Wang, Z. Jia, X. Qi, H. Zhu, X. Liu, Nanoparticle-stabilized foam with controllable structure for enhanced foamed concrete, *Constr. Build. Mater.* 362 (2023) 129723, <https://doi.org/10.1016/j.conbuildmat.2022.129723>.
- [42] N. Song, Z. Li, S. Wang, G. Li, Preparation of biomass carbon dots for foam stabilizer of foamed concrete, *Constr. Build. Mater.* 364 (2023) 129853, <https://doi.org/10.1016/j.conbuildmat.2022.129853>.
- [43] K.H. Yang, J.H. Mun, S.J. Kwon, J.W. Kim, Development of foam-concrete granules coated with TiO₂ nanoparticles, *Acids Mater. J.* 120 (2023) 3–18, <https://doi.org/10.14359/51738507>.
- [44] M.A.O. Mydin, M.N.M. Nawi, R. Omar, M.A. Khadimallah, I.M. Ali, R. Deraman, The use of inorganic ferrous-ferric oxide nanoparticles to improve fresh and durability properties of foamed concrete, *Chemosphere* 317 (2023) 137661, <https://doi.org/10.1016/j.chemosphere.2022.137661>.
- [45] M.A.O. Mydin, M.N. Mohd Nawi, O. Mohamed, M.W. Sari, Mechanical properties of lightweight foamed concrete modified with magnetite (Fe₃O₄) nanoparticles, *Mater. (Basel)* 15 (2022) 5911, <https://doi.org/10.3390/ma15175911>.
- [46] N. Song, Z. Li, W. Yi, S. Wang, Properties of foam concrete with hydrophobic starch nanoparticles as foam stabilizer, *J. Build. Eng.* 56 (2022) 104811, <https://doi.org/10.1016/j.jobe.2022.104811>.
- [47] J.P. Hidalgo, S. Welch, J.L. Torero, Performance criteria for the fire safe use of thermal insulation in buildings, *Constr. Build. Mater.* 100 (2015) 285–297, <https://doi.org/10.1016/j.conbuildmat.2015.10.014>.
- [48] G. Xian, Z. Liu, Z. Wang, X. Zhou, Study on the performance and mechanisms of high-performance foamed concrete, *Mater. (Basel)* 15 (2022) 7894, <https://doi.org/10.3390/ma15227894>.
- [49] Z.G. Cui, Y.Z. Cui, C.F. Cui, Z. Chen, B.P. Binks, Aqueous foams stabilized by in situ surface activation of CaCO₃ nanoparticles via adsorption of anionic surfactant, *Langmuir* 26 (2010) 12567–12574, <https://doi.org/10.1021/la1016559>.
- [50] A.G. Mehairi, M.M. Husein, Enhancement of cement properties by means of in situ grown nanoparticles, *Constr. Build. Mater.* 261 (2020) 120496, <https://doi.org/10.1016/j.conbuildmat.2020.120496>.
- [51] M. Cao, X. Ming, K. He, L. Li, S. Shen, Effect of macro-, micro- and nano-calcium carbonate on properties of cementitious composites-a review, *Mater. (Basel)* 12 (2019) 781, <https://doi.org/10.3390/ma12050781>.
- [52] S.S. Sahu, I.S.R. Gandhi, S. Khwairakpam, State-of-the-art review on the characteristics of surfactants and foam from foam concrete perspective, *J. Inst. Eng. Ser. A* 99 (2018) 391–405, <https://doi.org/10.1007/s40030-018-0288-5>.
- [53] G. Li, H. Tan, X. He, J. Zhang, X. Deng, Z. Zheng, Research on the properties of wet-ground waste limestone powder as foam stabilizer in foamed concrete, *Constr. Build. Mater.* 329 (2022) 127203, <https://doi.org/10.1016/j.conbuildmat.2022.127203>.
- [54] X. Ta, Z. Wan, Y. Zhang, S. Qin, J. Zhou, Effect of carbonation and foam content on CO₂ foamed concrete behavior, *J. Mater. Res. Technol.* 23 (2023) 6014–6022, <https://doi.org/10.1016/j.jmrt.2023.02.178>.
- [55] X. Ta, Y. Zhang, Z. Wan, P. Shi, J. Zhou, Study on preparation and performance of CO₂ foamed concrete for heat insulation and carbon storage, *Mater. (Basel)* 16 (2023) 2725, <https://doi.org/https://doi.org/10.3390/ma16072725>.
- [56] T. Li, F. Huang, J. Zhu, J. Tang, J. Liu, Effect of foaming gas and cement type on the thermal conductivity of foamed concrete, *Constr. Build. Mater.* 231 (2020) 117197, <https://doi.org/10.1016/j.conbuildmat.2019.117197>.
- [57] J. Bang, Y. Nam, W. Kim, K. Sun, C. Wan, S. Chun, S. Lee, S. Park, M. Gyu, Precipitation of calcium carbonate by carbon dioxide microbubbles, *Chem. Eng. J.* 174 (2011) 413–420, <https://doi.org/10.1016/j.cej.2011.09.021>.
- [58] A.G. Mehairi, R. Khoshnazar, M.M. Husein, Stability of CO₂/N2 foam generated in CaCO₃ nanoparticle/CTAB aqueous dispersion, *Chem. Eng. Sci.* 286 (2024) 119643, <https://doi.org/10.1016/j.ces.2023.119643>.
- [59] ASTM, C495/C495M: Standard Test Method for Compressive Strength of Lightweight Insulating Concrete, (2019) 1–3. https://doi.org/10.1520/C0495_C0495M_12R19.
- [60] ASTM, C796/C796M: Standard Test Method for Foaming Agents for Use in Producing Cellular Concrete Using Preformed Foam, (2019) 1–6. https://doi.org/10.1520/C0796_C0796M-19.
- [61] K. Scrivener, R. Snellings, B. Lothenbach, *A Practical Guide to Microstructural Analysis of Cementitious Materials*, CRC Press, 2016.
- [62] K. Jangir, U. Kumar, N.K. Suniya, N. Singh, K. Parihar, Enhancing the aqueous foam stability using nanoparticles: a review, *World J. Chem. Educ.* 10 (2022) 84–90, <https://doi.org/10.12691/wjce-10-2-5>.
- [63] D.L. Weaire, S. Hutzler, *The Physics of Foams*, Oxford University Press, Oxford, 1999.
- [64] R.J. Pugh, The stability / instability of bubbles and foams, in: *Bubble Foam Chem*, Cambridge University Press, Cambridge, 2016, pp. 220–268, <https://doi.org/10.1017/CBO9781316106938.008>.
- [65] R.J. Pugh, Basic principles and concepts, in: *Bubble Foam Chem*, Cambridge University Press, Cambridge, 2016, pp. 1–53, <https://doi.org/10.1017/cbo9781316106938.002>.
- [66] R.J. Pugh, Processes in foaming, in: *Bubble Foam Chem*, Cambridge University Press, Cambridge, 2016, pp. 112–154.
- [67] R.J. Pugh, Generation of bubbles and foams, in: *Bubble Foam Chem*, Cambridge University Press, Cambridge, 2016, pp. 155–193, <https://doi.org/10.1017/CBO9781316106938.006>.
- [68] G. Gu, F. Xu, X. Huang, S. Ruan, C. Peng, J. Lin, Foamed geopolymers: the relationship between rheological properties of geopolymers paste and pore-formation mechanism, *J. Clean. Prod.* 277 (2020) 123238, <https://doi.org/10.1016/j.jclepro.2020.123238>.
- [69] Z. Liu, K. Zhao, C. Hu, Y. Tang, Effect of water-cement ratio on pore structure and strength of foam concrete, *Adv. Mater. Sci. Eng.* 2016 (2016) 9520294, <https://doi.org/10.1155/2016/9520294>.
- [70] E.P. Kearsley, P.J. Wainwright, Porosity and permeability of foamed concrete, *Cem. Concr. Res.* 31 (2001) 805–812, [https://doi.org/10.1016/S0008-8846\(01\)00490-2](https://doi.org/10.1016/S0008-8846(01)00490-2).
- [71] Q. Fu, Z. Zhang, X. Zhao, W. Xu, D. Niu, Effect of nano calcium carbonate on hydration characteristics and microstructure of cement-based materials: a review, *J. Build. Eng.* 50 (2022) 104220, <https://doi.org/10.1016/j.jobe.2022.104220>.
- [72] A. Ipavec, R. Gabrošek, T. Vuk, V. Kaucić, J. Maček, A. Meden, Carboaluminates phases formation during the hydration of calcite-containing, *Portland Cem. J. Am. Ceram. Soc.* 94 (2011) 1238–1242, <https://doi.org/10.1111/j.1551-2916.2010.04201.x>.